JAERI-M
82-046

EXPERIMENTAL RESULTS ON ICRF HEATING IN JFT-2

May 1982

H. KIMURA, H. MATSUMOTO, K. ODAJIMA,
S. KONOSHIMA, N. SUZUKI, T. YAMAMOTO,
K. HOSHINO, Y. MIURA, T. MATSUDA,
H. TAKEUCHI, T. SUGIE, S. KASAI,
T. YAMAUCHI, H. KAWASHIMA, T. MATOBA,
T. OGAWA, T. KAWAKAMI, T. SHOJI, M. MORI
K. OHASA, S. YAMAMOTO, M. MAENO,
S. SENGOKU, H. NAKAMURA and H. OHTSUKA

日 本 原 子 力 研 究 所
Japan Atomic Energy Research Institute

JAERI-M レポートは，日本原子力研究所が不定期に公刊している研究報告書です。

入手の問合わせは，日本原子力研究所技術情報部情報資料課（〒319—11 茨城県那珂郡東海村）あて，お申しこしください。なお，このほかに財団法人原子力弘済会資料センター（〒319—11 茨城県那珂郡東海村日本原子力研究所内）で複写による実費頒布をおこなっております。

JAERI-M reports are issued irregularly.

Inquiries about availability of the reports should be addressed to Information Section, Division of Technical Information, Japan Atomic Energy Research Institute, Tokai-mura, Naka-gun, Ibaraki-ken 319—11, Japan.

編集兼発行　日本原子力研究所
印　　刷　日立高速印刷株式会社

JAERI-M 82-046

Experimental Results on ICRF Heating in JFT-2

Haruyuki KIMURA, Hiroshi MATSUMOTO, Kazuo ODAJIMA,
Shigeru KONOSHIMA+, Norio SUZUKI, Takumi YAMAMOTO,
Katsumichi HOSHINO, Yukitoshi MIURA, Toshiaki MATSUDA+,
Hiroshi TAKEUCHI+, Tatsuo SUGIE+, Satoshi KASAI,
Toshihiko YAMAUCHI, Hisato KAWASHIMA, Tohru MATOBA,
Toshihide OGAWA, Tomohide KAWAKAMI, Teruaki SHOJI,
Masahiro MORI, Kazumi OHASA+, Shin YAMAMOTO, Masaki MAENO,
Seio SENGOKU, Hiroo NAKAMURA+ and Hidewo OHTSUKA

Division of Thermonuclear Fusion Research,
Tokai Research Establishment, JAERI

(Received April 21, 1982)

600 kW of ICRF power is coupled to the JFT-2 plasma from the high field side using small area antennae (460 cm^2). By the net input of 500 kW, ion temperature increases from 0.4 to 0.8 keV, that of electron 0.6 to 0.9 keV, and the increment of β_p is $0.35 \sim 0.4$. The heating mechanism changes with the ratio of minority H species in D plasma (n_H/n_D), but clear dependence on the n_H/n_D is not observed for the heating efficiency. Deuterium high energy tail is observed, which indicates direct absorption of the RF power by the majority deuterium.

Keywords; ICRF Heating, JFT-2, Ion Temperature Deuterium,
High Energy Tail.

+) Division of Large Tokamak Development, Tokai Research Establishment, JAERI

ＪＦＴ－２におけるＩＣＲＦ加熱実験の結果

日本原子力研究所東海研究所核融合研究部

木村　晴行・松本　宏・小田島和男・木島　滋[+]
鈴木　紀夫・山本　巧・星野　克道・三浦　幸敏
松田　俊明[+]・竹内　浩[+]・杉江　達夫[+]・河西　敏
山内　俊彦・川島　寿人・的場　徹・小川　俊英
河上　知秀・荘司　昭朗・森　雅博・大麻　和美[+]
山本　新・前野　勝樹・仙石　盛夫・中村　博雄[+]
大塚　英男

（１９８２年４月２１日受理）

６００kWまでのＩＣＲＦ加熱パワーを小面積のアンテナ（４６０cm^2）を用いて強磁場側よりＪＦＴ－２プラズマに結合させた。P_{Net}＝５００kWに対して，イオン温度及び電子温度は各々0.4 keVから0.８keVへ，0.６keVから0.９keVに上昇した。β_pの増加分は0.３５～0.４である。加熱機構はn_H/n_Dとともに変化するが，加熱効率に対するn_H/n_Dの明瞭な依存性は観測されなかった。重水素の高エネルギーテールが観測された。これは高周波パワーが主成分である重水素に直接吸収されたことを示している。

＋）　大型トカマク開発部

Contents

目　　次

1. Introduction

Ion cyclotron range of frequency (ICRF) heating is promising for heating tokamak plasmas.

The merits of ICRF heating are considered as follows: The heating mechanism is relatively simple and bulk plasma heating is possible. The upper limit of the electron density does not exist. These merits are quite suitable in applying the ICRF heating to a tokamak reactor.

Intensive investigations are now under way in order to demonstrate the ICRF heating in the much higher temperature and much denser density with the power level up to 2 MW [1, 2]. At present a loop antenna is used as a coupling structure. After the successful achievement of the high power ICRF heating in the medium size device, development of a reliable coupling structure will be a pressing issue in the next-generation large device.

In JAERI, ICRF heating experiment started in 1978 using JFT-2a/DIVA tokamak device with the RF power of 200 kW. In the DIVA experiment, optimization of the lower field side excitation was investigated and the excellent heating efficiency was obtained [3∿5].

This paper describes experimental results of the ICRF heating in the JFT-2 tokamak device with the RF power level of 1 MW.

The main objectives of the ICRF heating experiment on JFT-2 are as follows.

(1) Investigation of the higher field side excitation.

In a deuteron plasma with a minority proton component, second harmonic cyclotron resonance layer, two-ion hybrid cut-off layer and two-ion hybrid resonance layer are formed from the low field side along the toroidal axia. The magnetosonic (fast) wave excited from the higher field side propagates to the plasma core and then heavily damped at the confluent region with the ion Bernstein wave, resulting in the plasma heating. The coupling with the ion Bernstein wave takes place at the two-ion hybrid resonance layer. It is theoretically predicted that the extent of the coupling and the power partitioning among species change with the proton-to-deuteron density ratio n_H/n_D, since the distance between the two-ion hybrid resonance layer and the cyclotron resonance layer is determined by n_H/n_D [6,7]. However, quantitative estimation

or even qualitative estimation in some case have not yet been done to the complicated physics involved there.

On the other hand, the fast wave excited from the lower field side encounters firstly with the two-ion hybrid cut-off layer, and the coupling with the ion Bernstein wave is less effective. In this case, the wave power is mainly absorbed by the minority proton component in the wide range of n_H/n_D as reported from PLT [2].

In this paper, we show the experimental results of the higher field side excitation in the wide range of the plasma parameters with the RF net power up to 500 kW.

(2) Establishment of the ICRF heating technology up to 1 MW in a single port [8].

There are few problems in the power source. The largest obstacle in increasing the RF power is the RF breakdown in the coupling structure and the transmission line. We use 1/4-loop antennae. One of the reasons why we use the 1/4-loop antenna is to reduce the voltage at the coil and the power feedthrough by shortening the antenna length. Antenna aging before experiment is not necessary in usual case.

In return, very high voltage is generated in the transmission line connecting the antenna and the stub tuners. We have suppressed the breakdown up to 45 kV in experiment and 51 kV in vacuum test using 4 7/8" coaxial line with SF_6 gas at 3 atmospheric pressure.

Scaling of the antenna loading resistance is indispensable in applying the ICRF heating to the next-generation large device. We show the parameter dependence of the loading resistance, which is well explained by the strong damping model [9].

(3) Comparison with the neutral beam injection (NBI) heating and high β/β_p study with combination heating

2 MW NBI heating system has already been installed in JFT-2 and high β plasma has been investigated [10∿12]. It is of importance to analyze results of both heating methods in the same machine and to compare advantages and disadvantages of them. From this, we can definitely conclude whether ICRF can take the place of NBI in future. In addition, we challenge much higher toroidal beta or poloidal beta values in

combination of both methods.

We will report on this subject in near future.

2. Experimental Set-up

2.1 JFT-2 and Diagnostics

JFT-2 is a tokamak with 0.9 m major radius and 0.25 m minor radius. Toroidal magnetic field is up to 15 kG and plasma current is 160 kA at maximum [10].

Figure 1 is the top view of JFT-2 and shows arrangement of various diagnostic instruments along with the position of the ICRF antennas and the beam lines of NBI.

The energy spectra of majority and minority ion species were measured with a E// B mass descriminating charge exchange neutral energy analyzer [13]. The radial profile of the ion temperature was measured with a Czerny-Terner mounting vacuum monochromator using T_i, O and C lines. The neutron flux was also monitored with a REM counter [14].

The spatial profiles of the electron temperature and density were measured with a laser scattering in a single shot [15].

The measurements of hydrogen to deuterium density ratio were cross-checked by the spectroscopy (H_α, D_α), the mass descriminating charge exchange neutral analysis during discharge, and the mass analysis of the residual gas after discharge.

2.2 RF Equipments

The RF generator is operated at 18 MHz which is a cyclotron frequency for proton with the toroidal magnetic field B_t = 11.8 kG. The output power of the generator which has a single TH 116 power triode is about 1 MW to the 50 Ω dummy load, and the pulse duration is up to 50 ms.

Figure 2 is a cross-sectional view of JFT-2 together with the antennas. Both inside and outside antennas are shown in this figure. Only the inside antennas are used in the present experiment. No ceramic insulator is used except at the power feedthrough. The central conductor is separated from the plasm by the double layer Faraday shield.

Detailed structure of the antenna are shown in Fig. 3. The central conductor made of copper is 48 mm in width and 3 mm in thickness. Distances from the central conductor to the return conductor and the inner Faraday shield is 20 mm and 7 mm, respectively. The return conductor is made of stainless-steel and 80 mm in width. Radial spacing

between the two layers of the Faraday shield is 3 mm. The element of the Faraday shield is 7 mm in width and 1 mm in thickness. Poloidal gaps between the elements are 3 mm. The inner layer was of stainless-steel and the outer one was of molybdenum. Recently, the surface of the latter has been coated with TiC in order to reduce the molybdenum influx into the plasma [16].

Fig. 4 depicts the antennas, transmission line and impedance matching system schematically. Two antennas are installed from the adjacent ports and are supplied with the RF power in phase. We also used top and bottom ports in the same toroidal section, and supplied the RF power to them in phase. In this case, the antennas act as half turn loop antenna. The loading resistance and the heating efficiency are not different from those of the toroidally separated two antennae case.

From the beginning of this experiment, we have frequently encountered with a RF breakdown at transmission lines, antennas and generator. Various countermeasures have been taken to overcome the breakdown. Power-up process of the available RF power is shown in Fig. 5. P_{RF} (○) is the transmitted power to the stub tuners. P_{Net} (●) is the one excluding circuit loss from P_{RF} (see Sec. 3.1). Up to now, the maximum P_{RF} has reached to 820 kW and the maximum P_{Net} is about 600 kW. The power densities on the antenna surface and in the vacuum feedthrough reach to 1.4 kW/cm^2 and 8.7 kW/cm^2, respectively. The maximum voltage at the transmission line (filled with 3 atm. of SF_6 gas) is 45 kV and up to 51 kV in the vacuum test.

3. Experimental Results

3.1 Antenna Loading Resistance

The loading resistance is determined by $R_A = P_{RF}/I^2_{rf}$, where I_{rf} is the current at the antenna measured by a small one turn coil behind the antenna as shown in Fig. 2. The absorbed power by plasma is determined by $P_{Net} = [(R_A - R_C)/R_A]P_{RF}$ where R_A and R_C are loading resistance with and without plasma, respectively.

The loading resistance is critically dependent on the plasma position as shown in Fig. 6. The value is about 1 Ω because of the short length of the antenna. The vacuum loading which includes a loss of transmission line, is $0.6 \sim 0.7$ for the RG-19U coaxial cable and 0.4 Ω for the SF-120 (4 7/8") coaxial line [8].

Inward shift of the plasma decreases the radius but the distance between the antenna and the plasma does not change. On the other hand, outward shift increases that distance. The solid line is a calculated value by ref. 9. Considering the antenna length 48 cm, it should be noted that the measured values well agree with the values predicted by calculation.

On the other hand, the loading resistance has weak dependence on the electron density and the minority-to-majority density ratio. Figure 7 shows the loading resistance as a function of the line average electron density $\bar{n}_e$ for various minority-to-majority density ratio. The loading resistance increases slowly with $\bar{n}_e$, which is again consistent with the calculation (solid line in Fig. 7).

3.2 Plasma Position Control

Plasma position control with a feedback system is used in the JFT-2, but in the start up phase of the RF heating, the position control by the feedback system is not sufficient to suppress outward shift due to increase of plasma pressure.

Thus, we use a preprogram to increase a current of the vertical field coil. Figure 8 shows the current as a function of RF power input, P_{Net}. The open circles indicate well controlled plasma and closed circles show a failure of the control. From this figure, it can be said that the energy content in the plasma increases in proportion to the RF net power.

The gradient of the open circles indicates a rough estimation of the heating efficiency with the assumption of constant current profile that is $\Delta\beta_p/P_{Net} = 0.5 \sim 0.6$/MW at $I_p = 140$ kA.

3.3 Parameter Survey

Parameter dependence studies such as n_H/n_D, $\bar{n}_e$, B_T surveys are performed in order to obtain general properties of the JFT-2 ICRF experiment. The experimental conditions are surveyed as followingly, $\bar{n}_e = 1.7 \sim 5.5 \times 10^{13}$ cm^{-3}, $B_T = 11$ kG $\sim$ 15 kG, $n_H/n_D = 2 \sim 30$ % and $I_p = 100 \sim 150$ kA for the fixed 18 MHz frequency.

A scan of the toroidal field indicates that the increase of ion temperature sharply peaked when the hybrid layer is in the plasma center as shown in Fig. 9. This observation is indirect evidence for a centrally peaked deposition profile. In this paper, the toroidal magnetic field is selected so as to keep the mode conversion layer in the center of the plasma, hereafter.

Mass sensitive charge exchange spectrums during low power RF heating are shown in Fig. 10. Deuterium spectra in these cases have no high energy tails up to E = 4 keV, and the temperature determined by the slope are around 500 eV. The temperature increase of deuteron normalized by P_{Net} and the average electron density as a function of n_H/n_D is shown in Fig. 11. This figure shows that the increase of the ion temperature is almost constant irrespectively of n_H/n_D.

On the other hand, hydrogen spectra reveal non-Maxwellian distribution characterized by the existence of a high energy tail. The heating power density to the minority protons near the plasma center is derived from fitting the proton energy spectra to the Fokker-Planck theory [17]. The calculated spectra are shown by solid line in Fig. 10. The slope of the tail is the largest in the case of $n_H/n_D \lesssim 0.03$, but the power deposition per unit volume is the largest at $n_H/n_D \sim 10\%$. The n_H/n_D - dependence of the heating power density to protons is shown in Fig. 12. If the majority deuterous are heated only through collisional transfer from the minority protons, the experimental observation that the increase of ion temperature in those cases are almost the same cannot be explained. Thus, we should conclude that a part of the RF power is absorbed directly by deuterium.

If the RF power is directly absorbed by deuterium, the spectrum of

deuterium exhibits a high energy tail as predicted by a Fokker-Planck theory including large Larmor radius effects. The example of the calculation by the 2-dimensional linear Fokker-Planck code is shown in Fig. 13(a).

Deuterium and hydrogen charge exchange spectra with high power and low density are shown in Fig. 13(b). Significant high energy tail, which is almost the same as that of hydrogen, is observed. This fact evidently shows that the RF power is directly absorbed by deuterium. The high energy tail in deuterium spectrum is clear in the case of low density, and n_H/n_D = 2∿4% and 30%. In the case of $n_H/n_D \sim 10\%$, appreciable high energy tail is not observed, which is consistent with the results mentioned above. In the case $n_H/n_D \sim 30\%$, the second harmonic cyclotron layer of deuteron (same as fundamental cyclotron layer of proton) lies in the vicinity of plasma edge. This experimental fact should be interpreted that the mode conversion layer enhances the second harmonic cyclotron damping. It should be noted that the RF power is directly absorbed by deuterium.

The mode conversion theory predicts that hydrogen concentration in a deuterium plasma n_H/n_D is a key parameter to determine the absorption mechanism. Figure 14 shows heating efficiency as a function of n_H/n_D in wide range of density $\bar{n}_e = 1.7 \sim 5.5 \times 10^{13} cm^{-3}$ and P_{Net} = 200 ∿ 500 kW. Because of day-by-day reproducibility and variation of other condition such as plasma current, the experimental points are rather spread.

A clear parameter dependence of heating efficiencies, $\Delta T_{io}\bar{n}_e/P_{Net}$ $(\Delta T_{io} + \Delta T_{eo})\bar{n}_e/P_{Net}$ was not observed. It can be said that the heating efficiency is almost constant irrespective of n_H/n_D.

In the low density case denoted by □, typically $\bar{n}_e \lesssim 2 \times 10^{13}$, the increases of ion and electron temperature are small compared with the same n_H/n_D cases, which may be due to large increase of impurities and/or charge exchange loss. The density dependence of the ion heating is shown in Fig. 15. For $\bar{n}_e \gtrsim 3 \times 10^{13}$ cm^{-3}, $\Delta T_i \cdot \bar{n}_e/P_{Net} \sim 4 \times 10^{13}$ $eV \cdot cm^{-3} \cdot kW^{-1}$ was obtained.

Finally, we show the power dependence of the ion heating for $3 \times 10^{13} \lesssim \bar{n}_e \lesssim 5 \times 10^{13}$ cm^{-3} and n_H/n_D = 2∿4% and ∿10%. The solid line corresponds to $\Delta T_i \cdot \bar{n}_e/P_{Net} = 4 \times 10^{13}$ $eV \cdot cm^{-3}$ kW^{-1}.

3.4 High Power Heating Results

In this section, heating results with $P_{net} \gtrsim 500$ kW are shown under the following conditions; $\bar{n}_e = 4 \sim 5 \times 10^{13}$ cm^{-3}, $I_p \approx 140$ kA, $n_H/n_D = 2 \sim 30\%$. Toroidal magnetic field is chosen so as to keep the hybrid layer near the center.

Figure 17(a) shows typical time evolution of ion and electron temperature at the center, and β_p in the case $n_H/n_D \approx 30\%$. The β_p is determined by magnetic probe measurement. Deuterium temperature measured by mass sensitive change exchange neutral analyzer increases from 0.4 keV to 0.8 keV, and the electron temperature on the axis increases from 0.6 keV to 0.9 keV.

From the profile measurement of electron temperature as shown in Fig. 17(b) and assuming the ion temperature profile $T_i(r) = T_{io}(1-r^2)^{1.5}$, the calculated thermal energy content β_p is $0.5 \sim 0.55$ for Joule heating phase and about $0.8 \sim 0.9$ for RF heating phase, which are shown by triangles in Fig. 17(a), assuming that current profile does not change. These values are consistent with the magnetic measurement.

Figure 17(c) is the deuterium and hydrogen charge exchange neutral spectra of this case. Appreciable high energy tail but smaller than that of hydrogen is observed in the deuterium charge exchange spectrum. This fact indicates a direct absorption of the RF power by deuterium.

Time evolutions of the plasma current, loop voltage, radiation loss measured by the bolometer and spectral line intensity of MoXIII are shown in Fig. 17(d).

The loop voltage including Li decreases from 2 volt before the RF to 1.1 V during the RF. The decrease of the loop voltage is consistent with the increase of electron temperature with the assumption of constant $Z_{ff}(\sim 1.8)$ and constant current profile. The decrease of Joule input during the RF is about 100 kW. Radiation loss measured by bolometer increases up to $2 \sim 2.5$ times as high as that of the Joul heating phase. Taking into account of the increase of the power input by a factor of about 3, the radiation loss does not fatally affect the energy balance.

Almost the same results are obtained in the case of $n_H/n_D = 2 \sim 4$ %. The profiles of ion and electron temperature are shown in Fig. 18. The radial position of the Doppler broadening temperature are determined by scanning the monochromator. The increase of β_p is 0.24, whose value is also consistent with the magnetic measurement. Significant increase of

ion and electron temperature are observed in a entire region of the plasma. But these profiles are more peaked than the Joule heating phase, which may be due to peaking of power deposition profile and increase of radiation loss. The radiation loss in this case increases 5 times as high as that of the Joule heating phase, but still the loop voltage decreases from 2 Volt to 1.5 Volt.

Comparing the both cases of $n_H/n_D \sim 30\%$ and $n_H/n_D = 2 \sim 4\%$, the electron temperature exceeds that of the ion by about 100 eV in the former case. In the latter case, however, the electron and ion temperature are almost the same. This difference becomes clearer in the low density case. The excess of electron temperature, about 200 eV is indirect indication of absorption of RF power by electrons. Computer simulation by 1-D tokamak code show that if all of the RF power deposits on ions, the ion and electron temperature are almost the same in high density case and the ion temperature exceeds the electron temperature in low density case. Therefore it can be said that the RF power deposits directly on electrons.

Figure 19 shows time evolutions of β_p measured by magnetics. Those two cases, $n_H/n_D = 2 \sim 4$ %, 30 %, show almost the same increase of β_p at power level $500 \sim 550$ kW, that is $\Delta\beta_p \approx 0.4$. The initial slope of $(d\beta_p/dt)_{t=0}$ when the RF is applied at power level $\sim$500 kW, we can obtain a lower limit of an effective heating power. If the slope is taken at initial 5 ms, these values are 380 kW for $n_H/n_D \sim 30$ %, and 450 kW for $n_H/n_D = 2 \sim 4$ %. Taking account of a rather lower value of the $\dot{\beta}_p$, roughly 80 % of net power is absorbed in the hot core.

In concluding this section, a good heating results are obtained irrespective of the key parameter n_H/n_D.

4. Conclusions and Discussions

ICRF heating have been performed in JFT-2 at power levels up to 600 kW with small area antennae of 460 cm^2 in total. The radiation power density on the antenna surface reaches 1.4 kW/cm^2. The radiation resistance of the each antenna is 1 Ω and quantitatively agree with strong damping model proposed by J. Adam [9].

The heating results obtained are summarized as followingly:

1. Clear dependence of heating efficiencies represented by $\Delta T_{io}\bar{n}_e/P_{Net}$, $(\Delta T_{io} + \Delta T_{eo})\bar{n}_e/P_{Net}$ are not observed in the region $n_H/n_D = 2 \sim 30$ %.
   In the DIVA experiment, a strong dependence of heating efficiency on n_H/n_D, that is peaked at $n_H/n_D \sim 10$ %, is observed [3].
   The difference of n_H/n_D dependence between the JFT-2 and DIVA ICRF experiment can be understood by the difference between the higher and lower field side excitation.
   Full wave equation for the mode conversion theory shows that almost all of the wave energy converts to the slow wave in the case of higher field side excitation [18].
2. Radiation loss does not fatally affect the energy balance in the high density case, on the otherhand, in the low density region ($\lesssim 2 \times 10^{13}$ cm^{-3}), impurity contamination is significant and the heating efficiency may decrease.
3. Around P_{Net} = 500 kW, ion temperature increases from 0.4 keV to 0.8 keV and that of electron from 0.6 keV to 0.9 keV are obtained at $\bar{n}_e = 4.5 \times 10^{13}$. Increase of the gross thermal energy $\Delta\beta_p$ is $0.35 \sim 0.4$. This value determined by magnetic measurement agrees well with the value obtained from profile measurement.

For the understanding of the heating mechanism, power distributions for each species of particles are matter of importance. The n_H/n_D scan shows the following results:

1. Preliminary power balance analysis indicates that the power deposition on minority hydrogen takes the maximum value at $n_H/n_D \sim 10$ % and in the case of the larger and smaller hydrogen concentrations than this, the RF power is dominantly absorbed by deuterium.
2. Deuterium high energy tails are observed at high power $P_{Net} \gtrsim 300$ kW. This fact is a clear evidence of the direct RF power absorption by

deuterium. Especially, in the case of $n_H/n_D \sim 30$ %, and B_T = 15 kG, the cyclotron layer lies in the vicinity of the plasma edge.

Up to now, there is no quantitative explanation of the direct absorption by deuterium. The experimental observations suggest that the mode conversion layer enhances the hamonic cyclotron damping.

3. Significant electron heating are observed in the case of $n_H/n_D \sim 30$ %.

Acknowledgements

The authors are grateful to the members of the JFT-2 and NBI operation groups for their excellent operations, especially to Messrs. M. Isaka and K. Kikuchi for their helpful supports in the construction of the RF generator. They are also indebted to Drs. S. Mori, Y. Iso, Y. Obata, M. Tanaka, Y. Tanaka and A. Funahashi for their continuous encouragements.

References

[1] TFR GROUP, EUR-CEA-FC-1108 (1981).

[2] HOSEA, J., BOYD, D., et al., in Plasma Physics and Controlled Nuclear Fusion Research, Brussels, 1980, IAEA-CN-38/D-5-1.

[3] KIMURA, H., ODAJIMA, K., et al., ibid IAEA-CN-38/D-5-2.

[4] IIZUKA, S., ODAJIMA, K., et al., Phys. Rev. Lett. 45 (1980) 1256.

[5] ODAJIMA, K., KIMURA, H., et al., Nucl. Fusion 20 (1980) 1331.

[6] COLESTOCK, P., DAVIS, S., et al., in 2nd Joint Varenna-Grenoble International Symposium on Heating in Toroidal Plasma Como, 1980, Vol. I.

[7] SWANSON, D., Nucl. Fusion 20 (1980) 949.

[8] JFT-2 GROUP., "Technical and Design Aspect of JFT-2 ICRF Heating", in 3rd Joint Varenna-Grenoble International Symposium on Heating in Toroidal Plasma Grenoble, 1982.

[9] ADAM, J., EUR-CEA-FC-1004 (1979).

[10] SUZUKI, N., IMAI, T., in Plasma Physics and Controlled Nucl. Fusion Research, Brussels, 1980, Vol. II 525.

[11] JFT-2 GROUP., Proc. 10th Europ. Conf. on Controlled Fusion and Plasma Phys., Moscow, 2 (1981).

deuterium. Especially, in the case of $n_H/n_D \sim 30$ %, and B_T = 15 kG, the cyclotron layer lies in the vicinity of the plasma edge.

Up to now, there is no quantitative explanation of the direct absorption by deuterium. The experimental observations suggest that the mode conversion layer enhances the hamonic cyclotron damping.

3. Significant electron heating are observed in the case of $n_H/n_D \sim 30$ %.

Acknowledgements

The authors are grateful to the members of the JFT-2 and NBI operation groups for their excellent operations, especially to Messrs. M. Isaka and K. Kikuchi for their helpful supports in the construction of the RF generator. They are also indebted to Drs. S. Mori, Y. Iso, Y. Obata, M. Tanaka, Y. Tanaka and A. Funahashi for their continuous encouragements.

References

[1] TFR GROUP, EUR-CEA-FC-1108 (1981).
[2] HOSEA, J., BOYD, D., et al., in Plasma Physics and Controlled Nuclear Fusion Research, Brussels, 1980, IAEA-CN-38/D-5-1.
[3] KIMURA, H., ODAJIMA, K., et al., ibid IAEA-CN-38/D-5-2.
[4] IIZUKA, S., ODAJIMA, K., et al., Phys. Rev. Lett. 45 (1980) 1256.
[5] ODAJIMA, K., KIMURA, H., et al., Nucl. Fusion 20 (1980) 1331.
[6] COLESTOCK, P., DAVIS, S., et al., in 2nd Joint Varenna-Grenoble International Symposium on Heating in Toroidal Plasma Como, 1980, Vol. I.
[7] SWANSON, D., Nucl. Fusion 20 (1980) 949.
[8] JFT-2 GROUP., "Technical and Design Aspect of JFT-2 ICRF Heating", in 3rd Joint Varenna-Grenoble International Symposium on Heating in Toroidal Plasma Grenoble, 1982.
[9] ADAM, J., EUR-CEA-FC-1004 (1979).
[10] SUZUKI, N., IMAI, T., in Plasma Physics and Controlled Nucl. Fusion Research, Brussels, 1980, Vol. II 525.
[11] JFT-2 GROUP., Proc. 10th Europ. Conf. on Controlled Fusion and Plasma Phys., Moscow, 2 (1981).

deuterium. Especially, in the case of $n_H/n_D \sim 30$ %, and B_T = 15 kG, the cyclotron layer lies in the vicinity of the plasma edge.

Up to now, there is no quantitative explanation of the direct absorption by deuterium. The experimental observations suggest that the mode conversion layer enhances the hamonic cyclotron damping.

3. Significant electron heating are observed in the case of $n_H/n_D \sim 30$ %.

Acknowledgements

The authors are grateful to the members of the JFT-2 and NBI operation groups for their excellent operations, especially to Messrs. M. Isaka and K. Kikuchi for their helpful supports in the construction of the RF generator. They are also indebted to Drs. S. Mori, Y. Iso, Y. Obata, M. Tanaka, Y. Tanaka and A. Funahashi for their continuous encouragements.

References

[1] TFR GROUP, EUR-CEA-FC-1108 (1981).
[2] HOSEA, J., BOYD, D., et al., in Plasma Physics and Controlled Nuclear Fusion Research, Brussels, 1980, IAEA-CN-38/D-5-1.
[3] KIMURA, H., ODAJIMA, K., et al., ibid IAEA-CN-38/D-5-2.
[4] IIZUKA, S., ODAJIMA, K., et al., Phys. Rev. Lett. 45 (1980) 1256.
[5] ODAJIMA, K., KIMURA, H., et al., Nucl. Fusion 20 (1980) 1331.
[6] COLESTOCK, P., DAVIS, S., et al., in 2nd Joint Varenna-Grenoble International Symposium on Heating in Toroidal Plasma Como, 1980, Vol. I.
[7] SWANSON, D., Nucl. Fusion 20 (1980) 949.
[8] JFT-2 GROUP., "Technical and Design Aspect of JFT-2 ICRF Heating", in 3rd Joint Varenna-Grenoble International Symposium on Heating in Toroidal Plasma Grenoble, 1982.
[9] ADAM, J., EUR-CEA-FC-1004 (1979).
[10] SUZUKI, N., IMAI, T., in Plasma Physics and Controlled Nucl. Fusion Research, Brussels, 1980, Vol. II 525.
[11] JFT-2 GROUP., Proc. 10th Europ. Conf. on Controlled Fusion and Plasma Phys., Moscow, 2 (1981).

[12] YAMAMOTO, S., MAENO, M., et al., Nucl. Fusion 21 (1981) 993.

[13] TAKEUCHI, H., et al., submitted to Reviw of Scientific Instrument.

[14] MATOBA, T., OGAWA, T., et al., to be published.

[15] YAMAUCHI, T., SANO, K., et al., Jpn. J. Appl. Phys. 21 (1982) 347.

[16] NAKAMURA, H., SENGOKU, S., et al., "TiC/Mo Faraday Shield and Carbon Limiter for Reduction of Metal Impurities in JFT-2 ICRF Plasmas", to be published in Japan Atomic Energy Research Institute Report JAERI-M (1982).

[17] STIX, T., Nucl. Fusion 15 (1975) 737.

[18] IIZUKA, S., ODAJIMA, K., et al., Japan Atomic Energy Research Institute Report JAERI-M 8595 (1979).

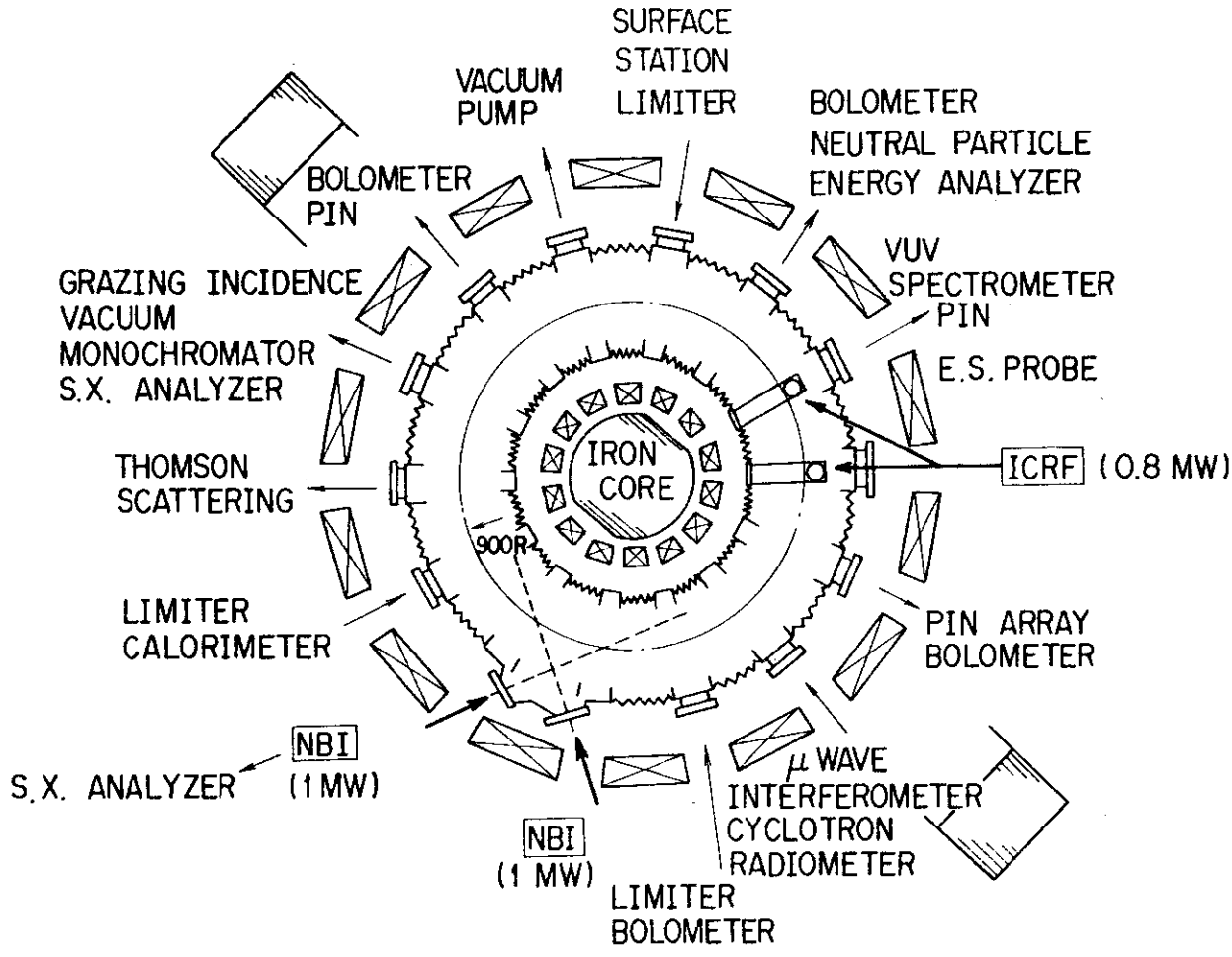

Fig. 1 Top view of JFT-2

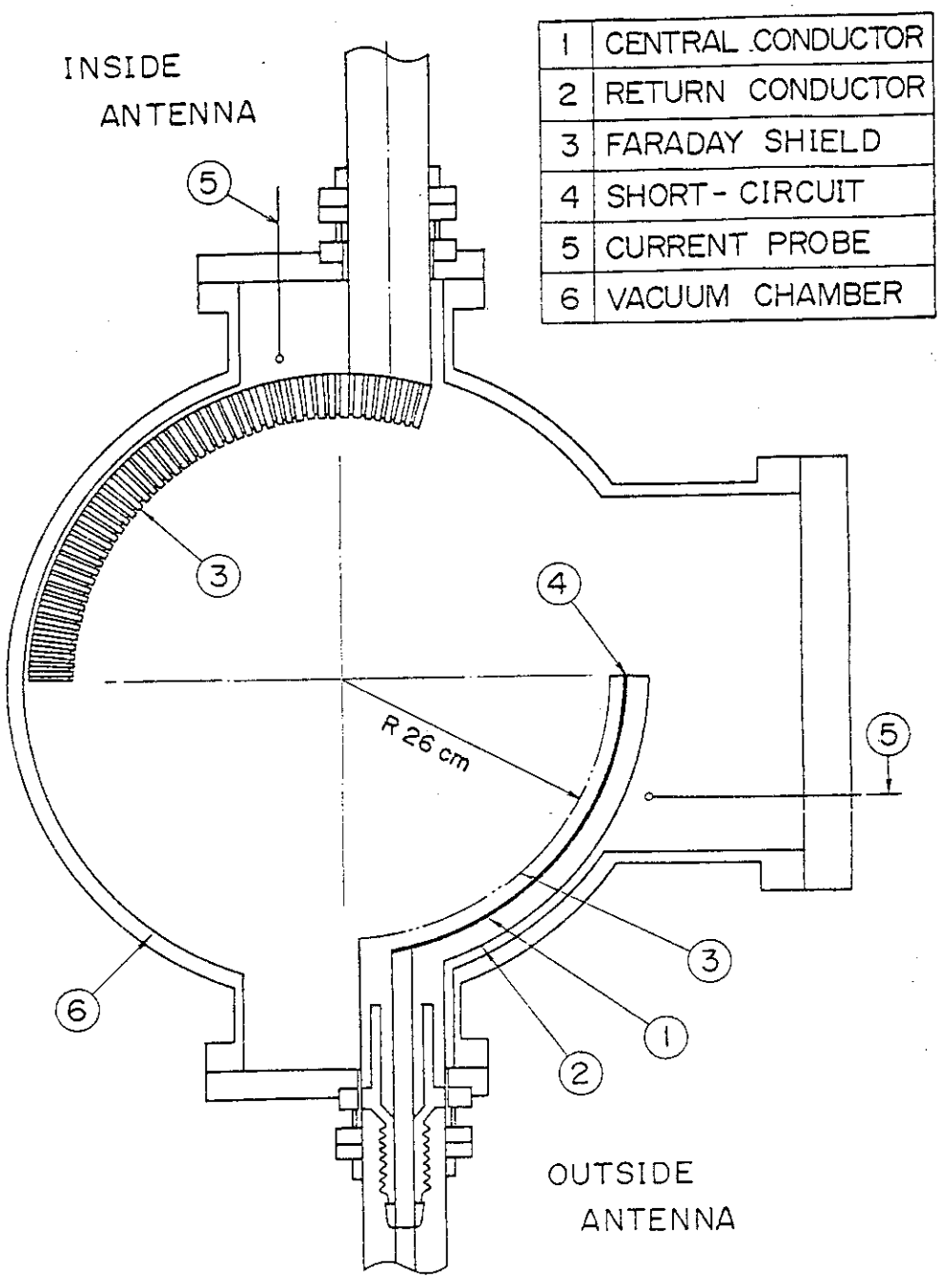

Fig. 2 Cross-sectional view of JFT-2 and all metal 1/4-loop antennae

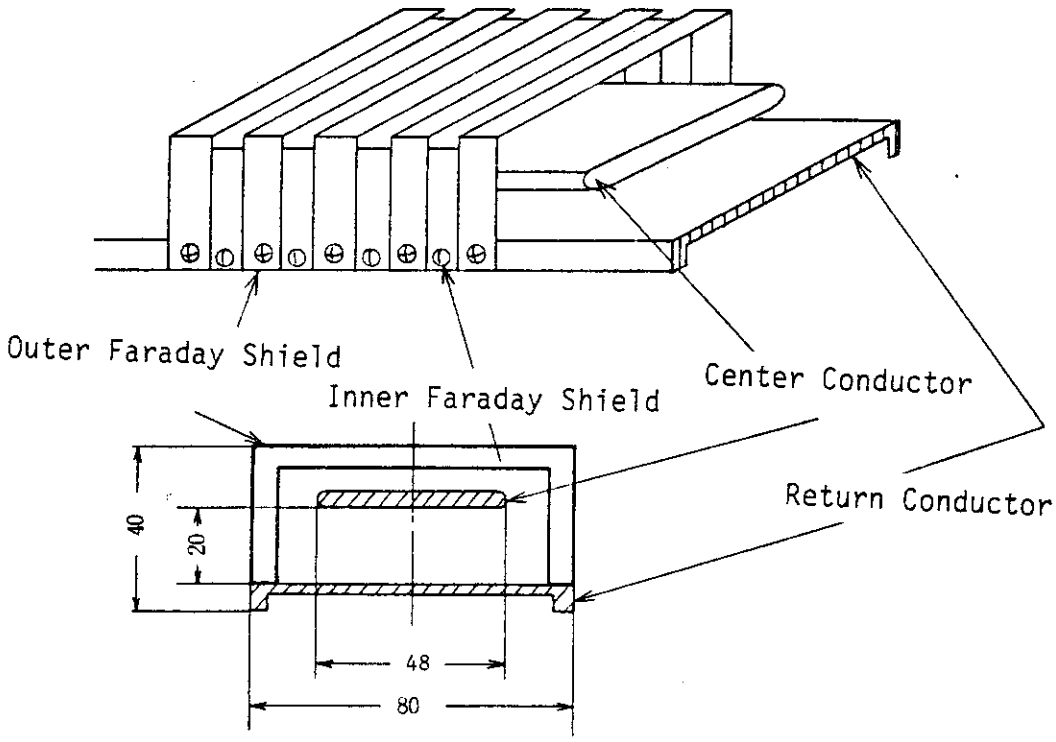

Fig. 3 Schematic drawing of antenna structure

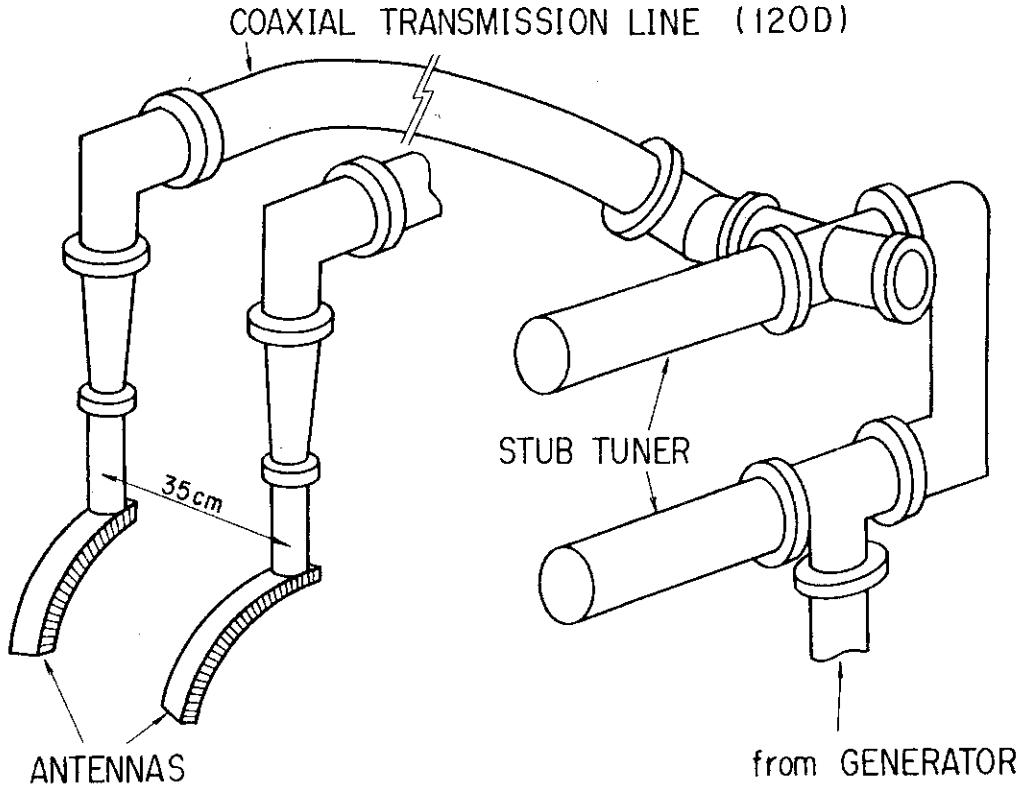

Fig. 4 Schematic drawing of antennas, transmission lines and stub tuners

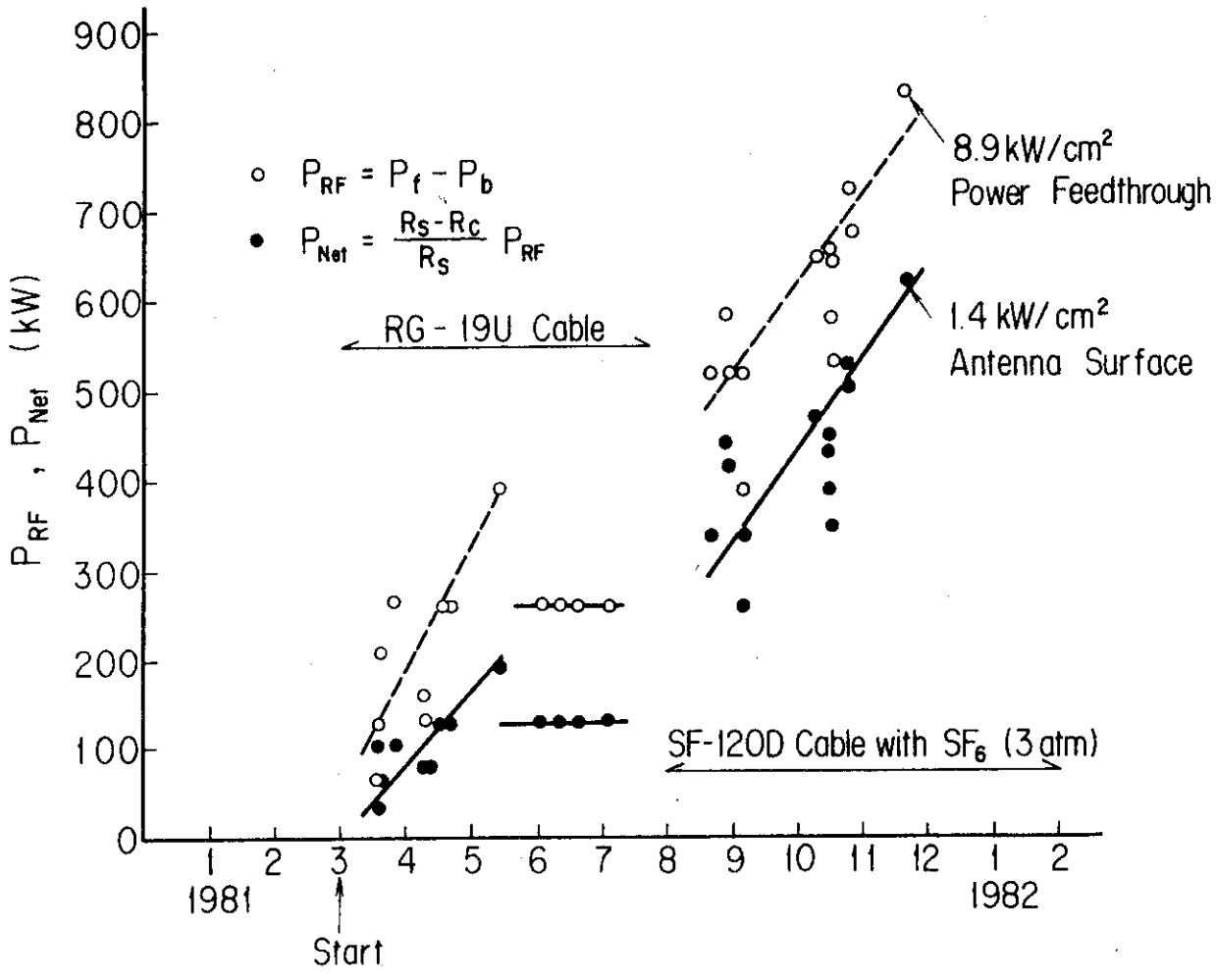

Fig. 5 Power-up process of the RF power as a function of a month. P_{RF}(○) is the transmitted power to the stub tuners and P_{Net}(●) is the one excluding the circuit loss from P_{RF}

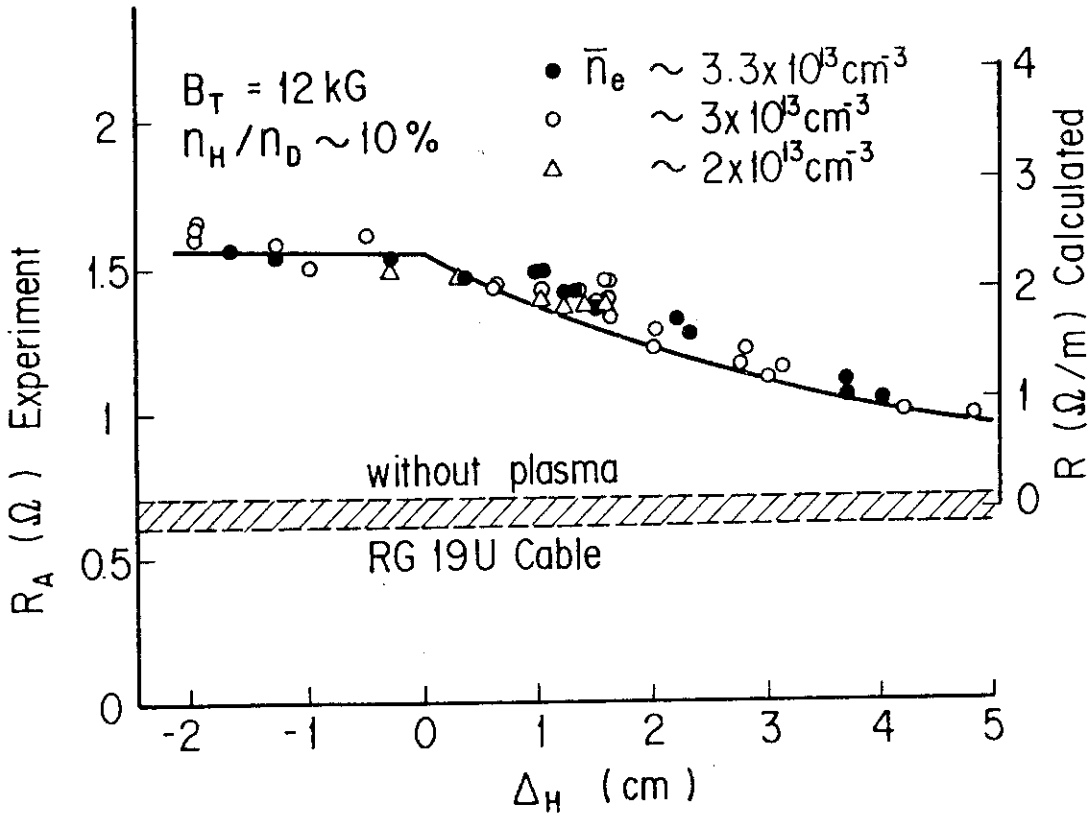

Fig. 6 Antenna loading resistance $R_A(\Omega)$ versus horizontal plasma position Δ_H(cm). Solid line is calculated value with the strong damping model [9]

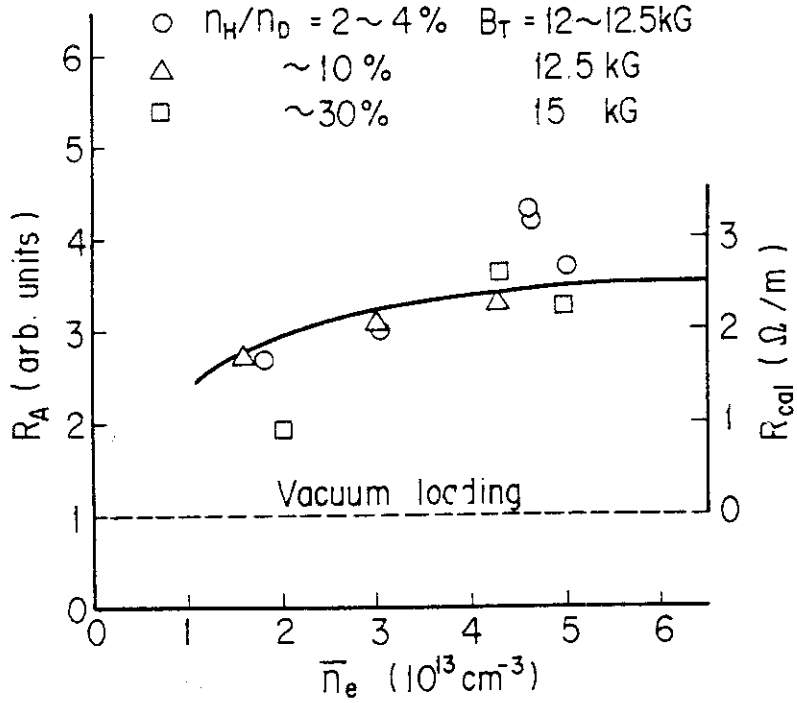

Fig. 7 Antenna loading resistance $R_A(\Omega)$ as a function of the line average electron density $\bar{n}_e$ for $2\% \lesssim n_H/n_D \lesssim 30\%$. Solid line is calculation for 100% D plasma

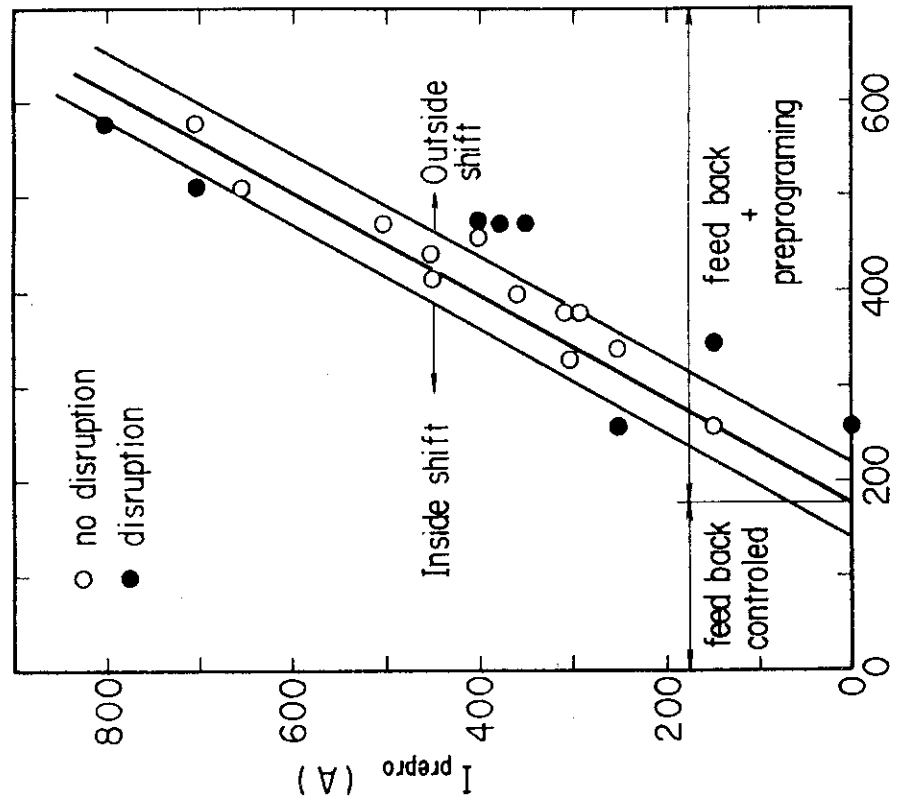

Fig. 8
Preprogrammed vertical coil current Iprepro (A) versus RF net power P_{Net}. The open circles indicate well controlled plasma and closed circles show failure of the control

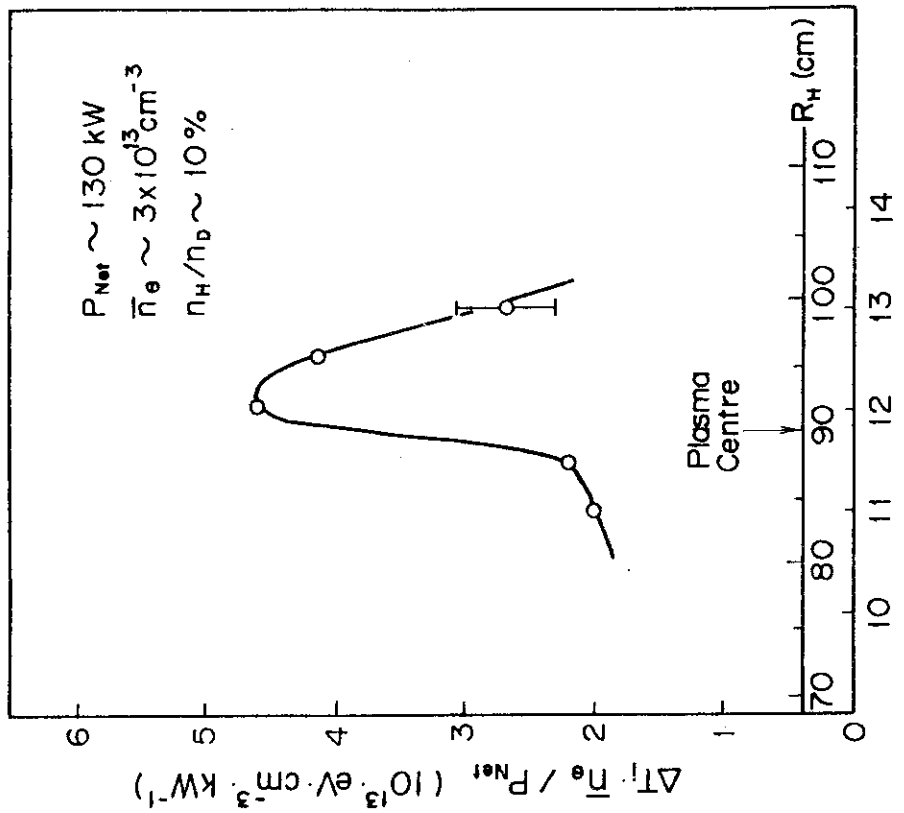

Fig. 9
B_T - dependence of the central ion temperature increase normalized by the RF net power and the average electron density. The proton-to-denteron density ratio $n_H/n_D \sim 10\%$

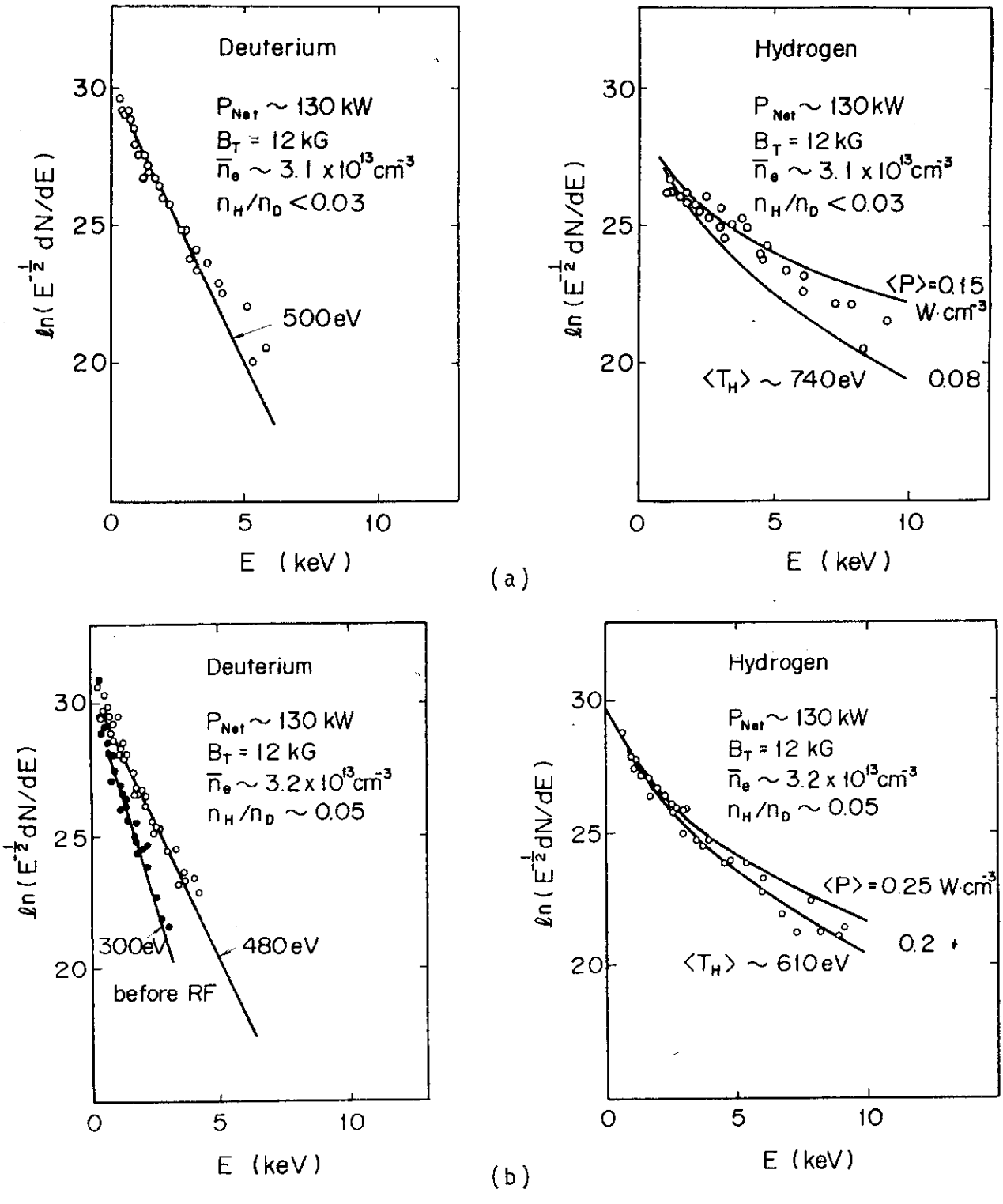

Fig. 10 Change exchange neutral spectra of deuterium and hydrogen during heating for various n_H/n_D.
(a) $n_H/n_D \leq 0.03$, (b) $n_H/n_D \sim 0.05$, (c) $n_H/n_D \sim 0.1$ and (d) $n_H/n_D \sim 0.2$. The fitting curves of the hydrogen spectra are calculated from the Fokker-Planck theory. The upper and lower limits of the local heating power density to protons <P> are shown in the figure

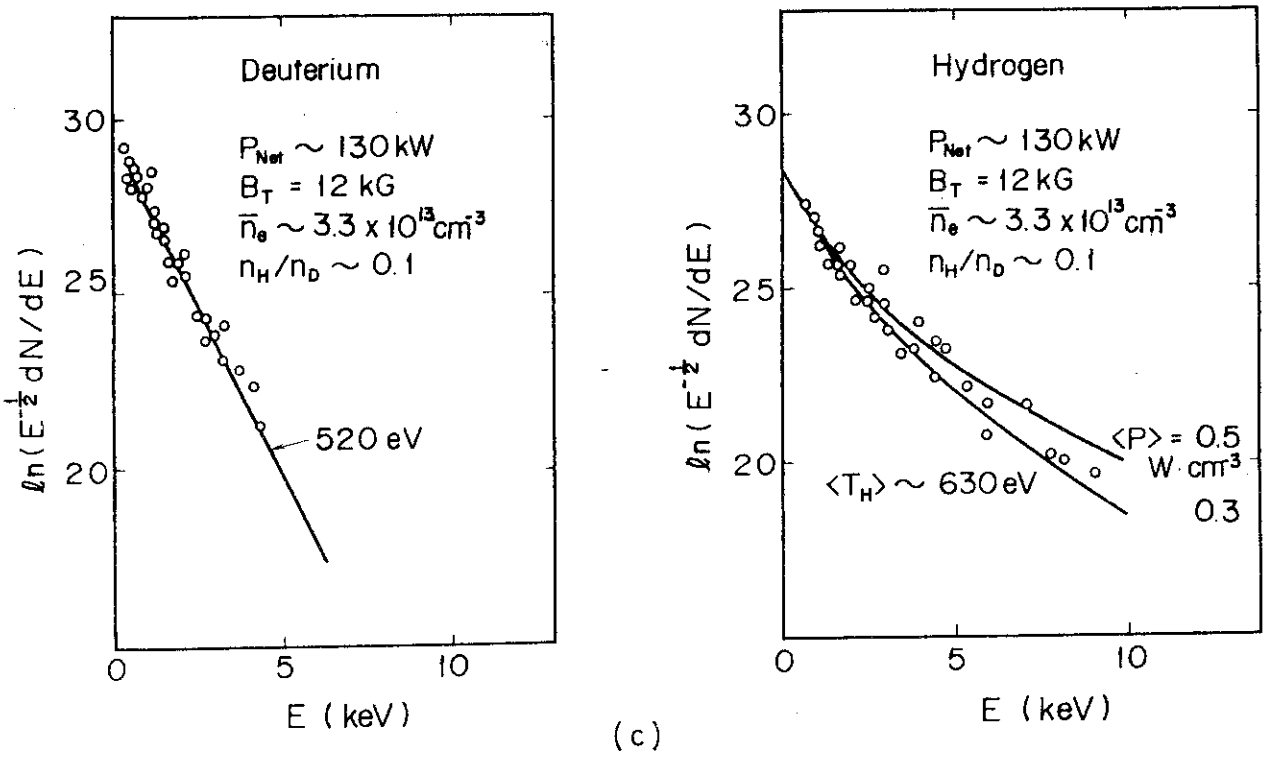

(c)

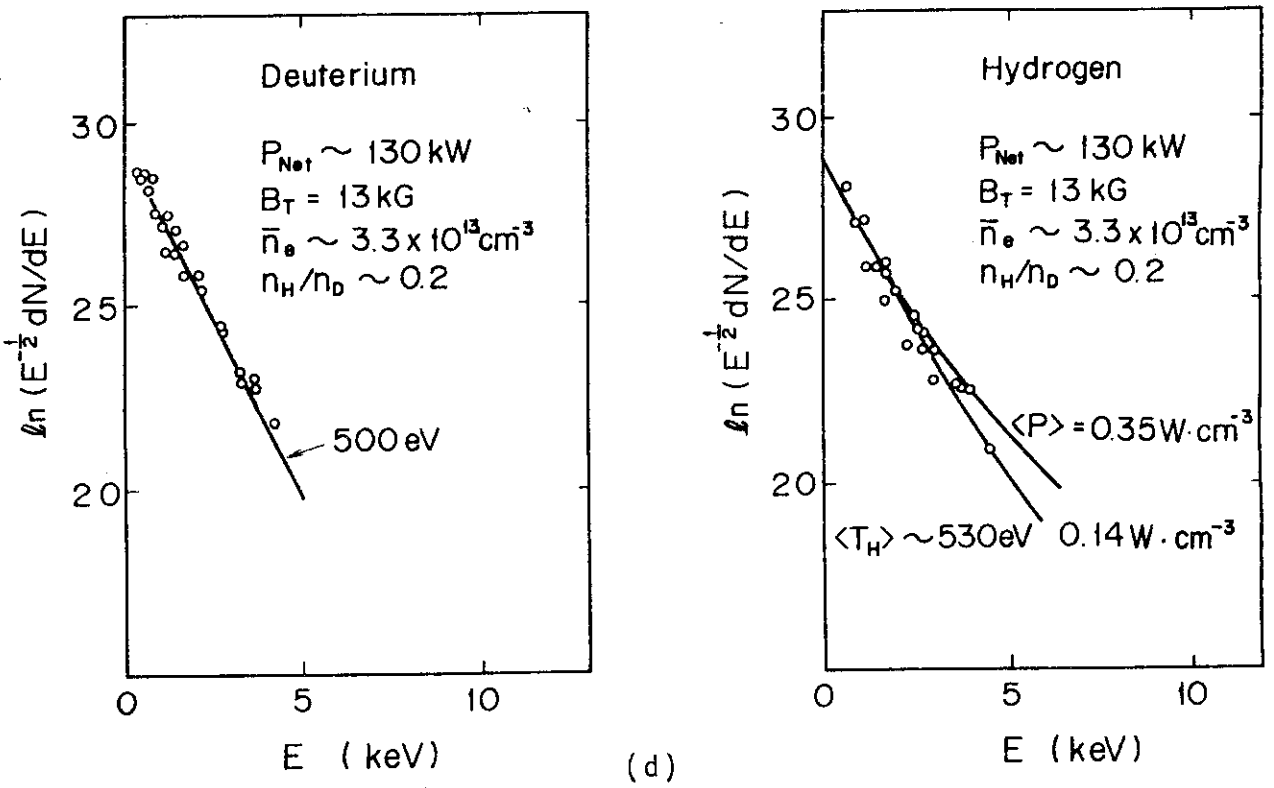

(d)

Fig. 10 (Continued)

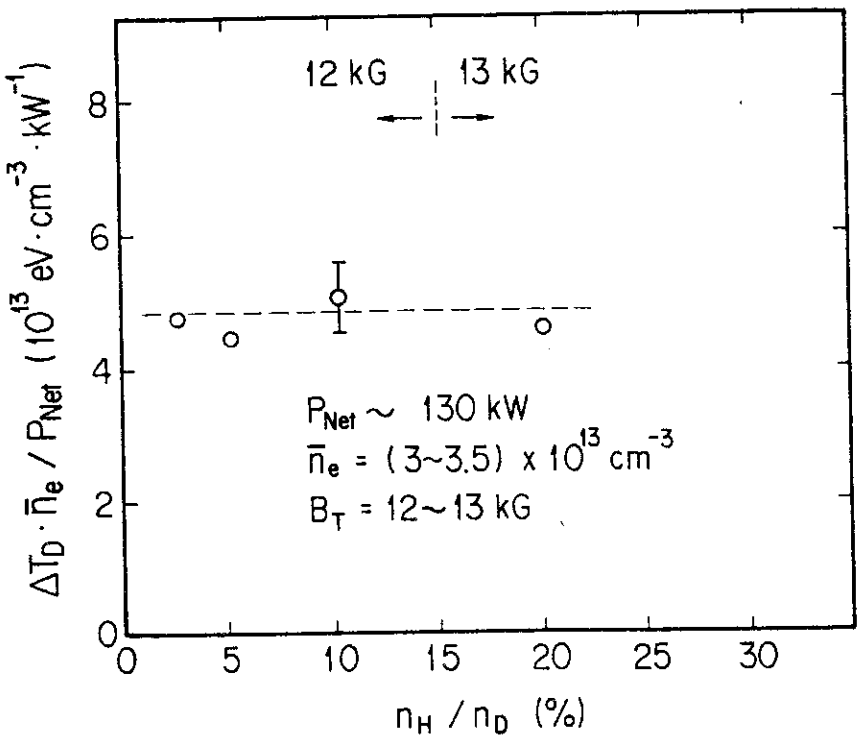

Fig. 11 n_H/n_D - dependence of the central ion temperature normalized by the RF net power and the average electron density

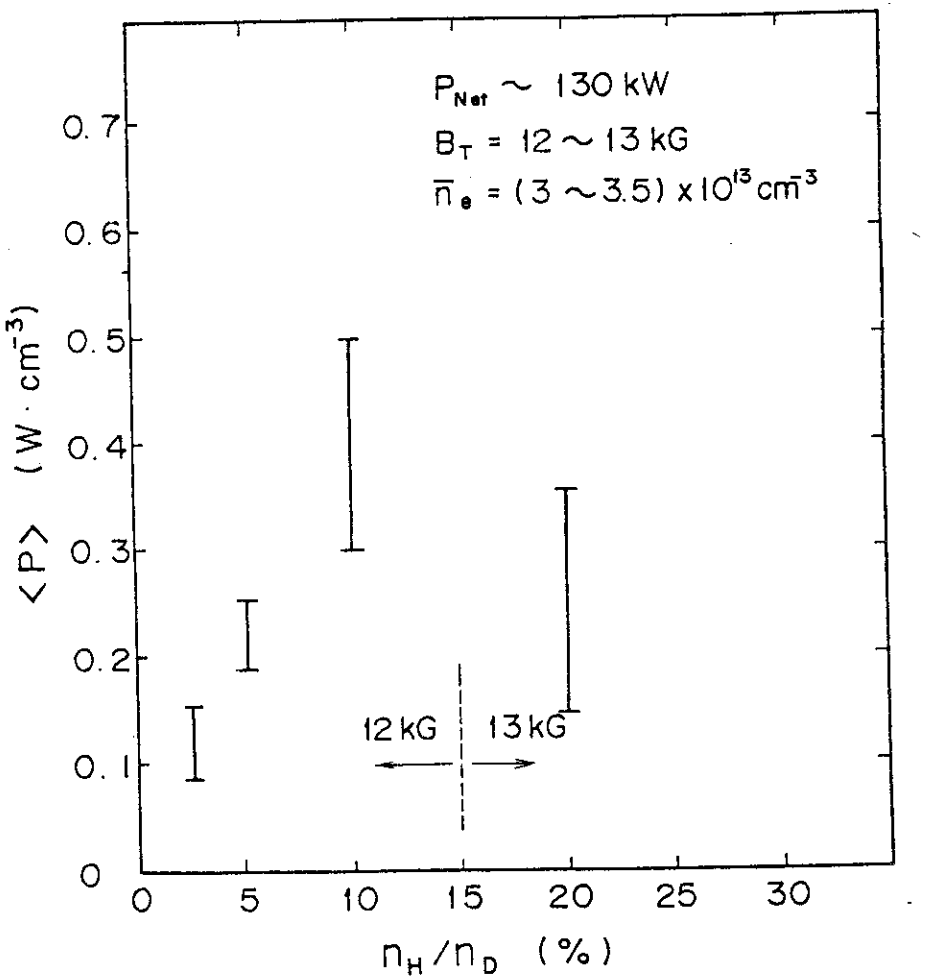

Fig. 12 n_H/n_D - dependence of the heating power density to the minority proton component corresponding to Fig. 11.

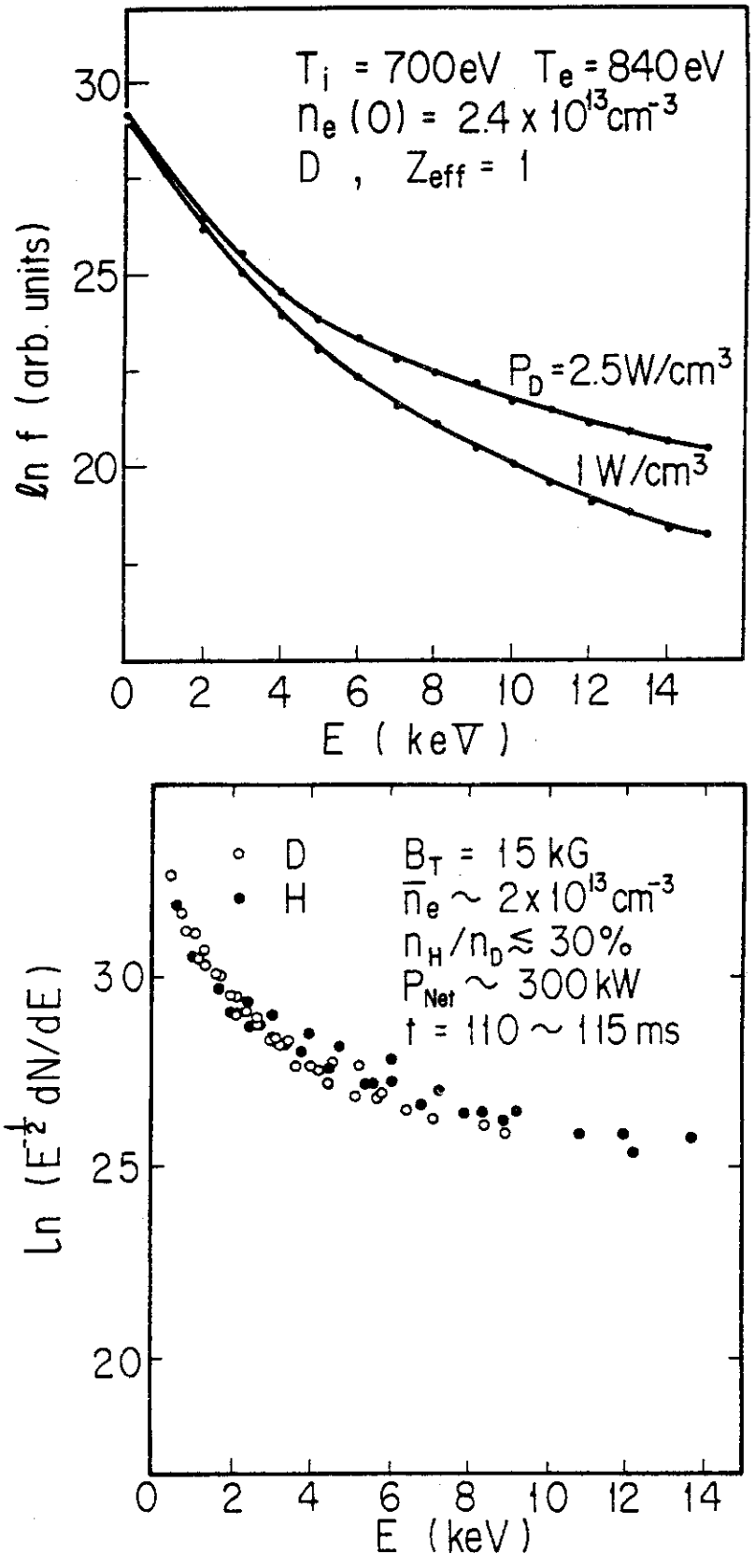

Fig. 13 (a) Calculation of the denterium energy spectrum for the second harmonic cyclotron heating on the basis of the two dimensional linear Fokker-Planck code.
(b) Deuterium and hydrogen charge exchange neutral energy spectra with high power and low electron density.

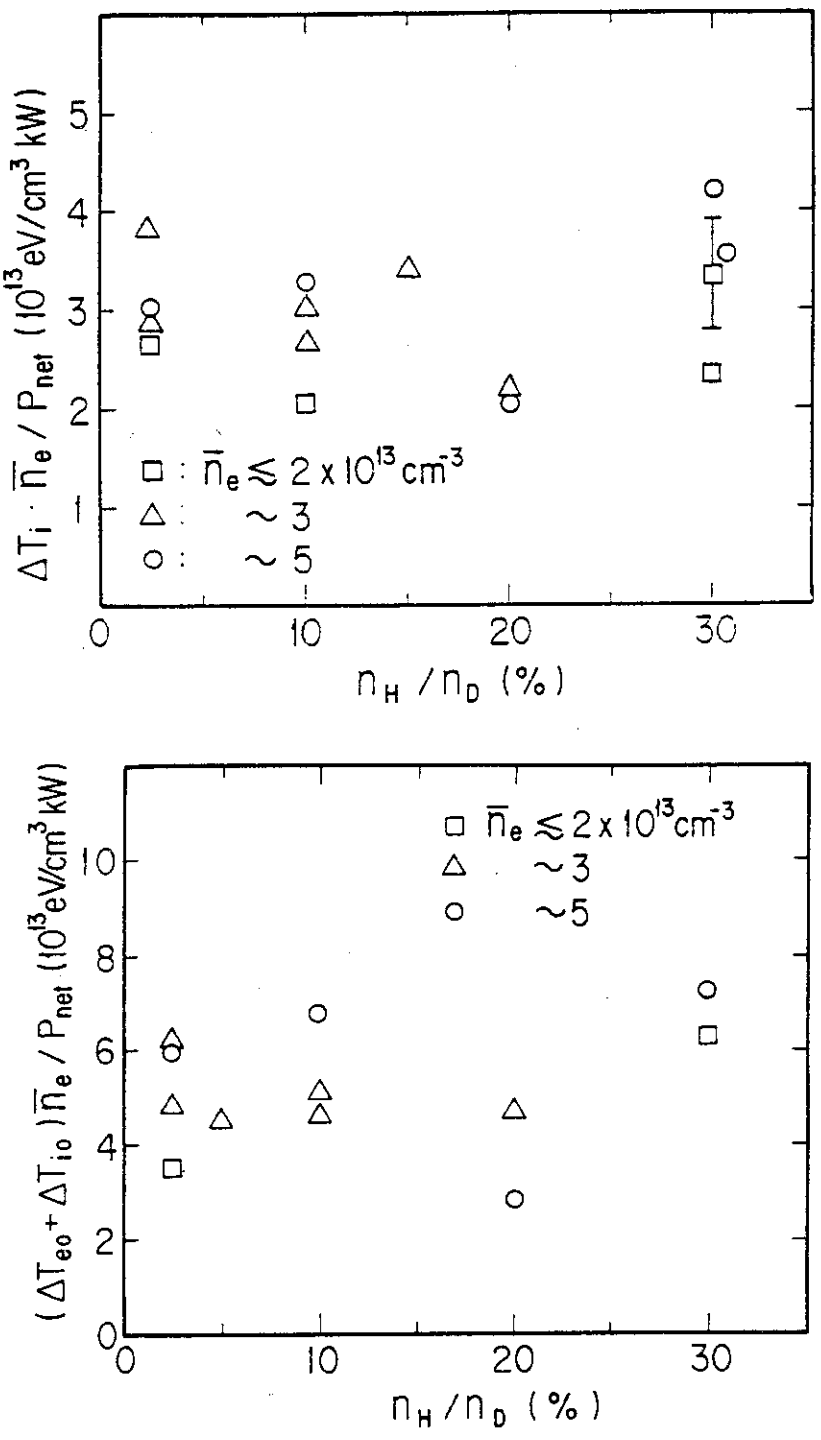

Fig. 14 (a) Ion heating efficiency $\Delta T_i \cdot \bar{n}_e / P_{Net}$ as a function of n_H/n_D with $\bar{n}_e = 1.7 \sim 5.5 \times 10^{13} cm^{-3}$ and $P_{Net} = 200 \sim 500$ kW. (b) Total heating efficiency $(\Delta T_i + \Delta T_e)\bar{n}_e / P_{Net}$ versus n_H/n_D.

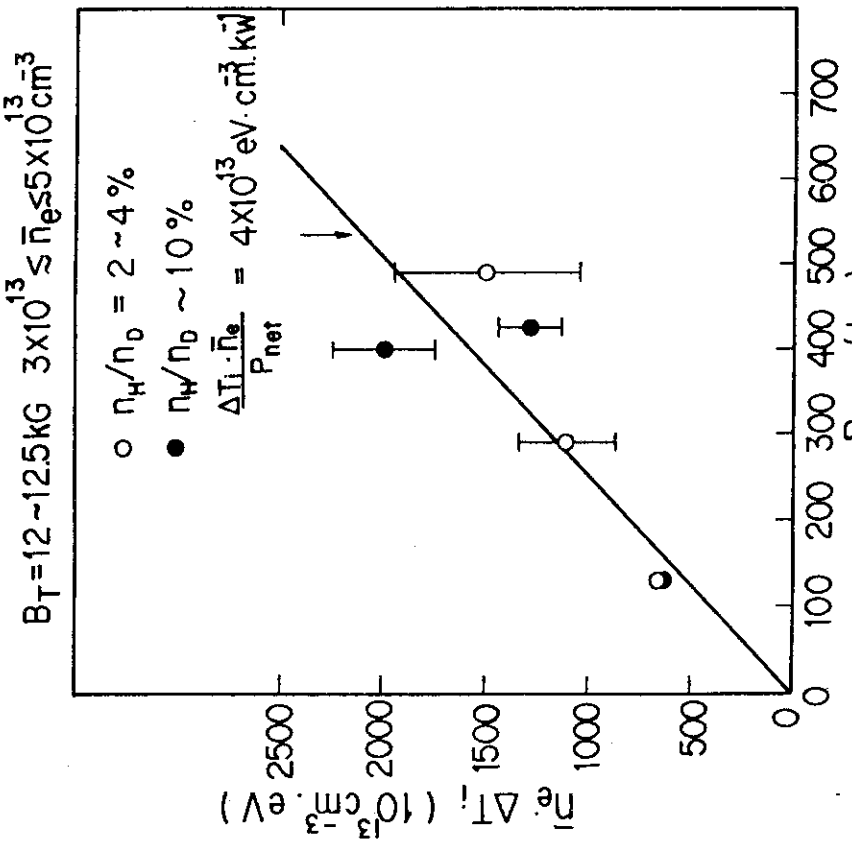

Fig. 16
$\bar{n}_e \cdot \Delta T_i$ versus P_{Net}. Open circles are n_H/n_D=2∿4% and closed ones are n_H/n_D∿10%. The solid line corresponds to $\Delta T_i \cdot \bar{n}_e/P_{Net}$=4×10^{13}eV·cm^{-3}·kW^{-1}.

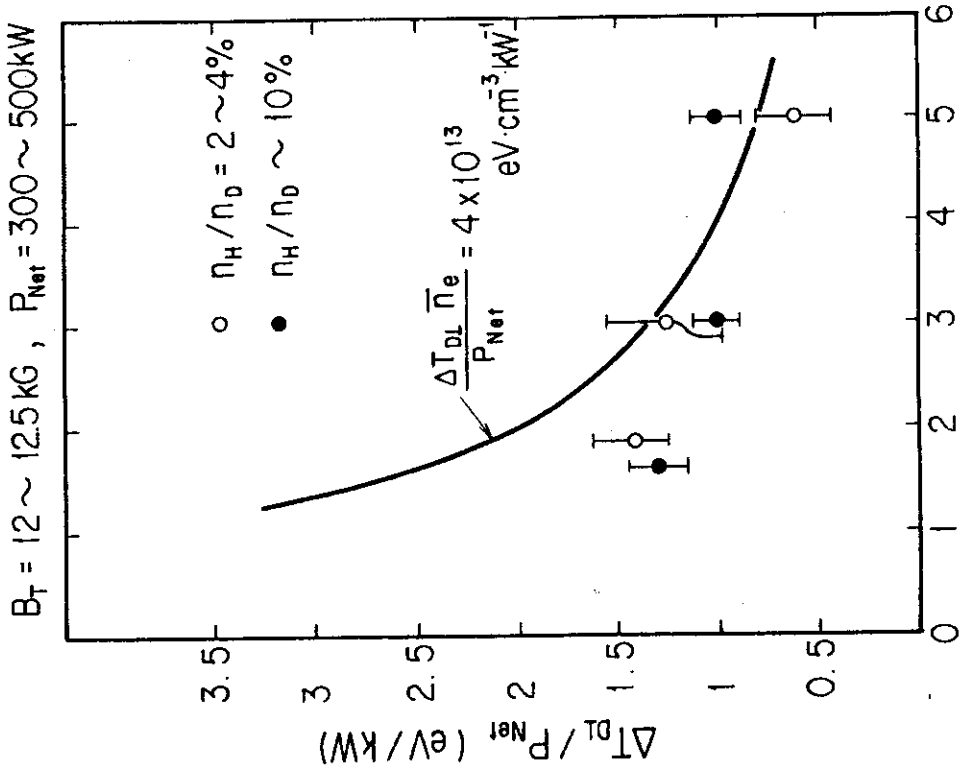

Fig. 15
$\Delta T_i/P_{Net}$ versus $\bar{n}_e$. Open circles are n_H/n_D=2∿4% and closed ones are n_H/n_D∿10%. The curve corresponds to $\Delta T_i \cdot \bar{n}_e/P_{Net}$ = 4 × 10^{13}eV·cm^{-3}·kW^{-1}.

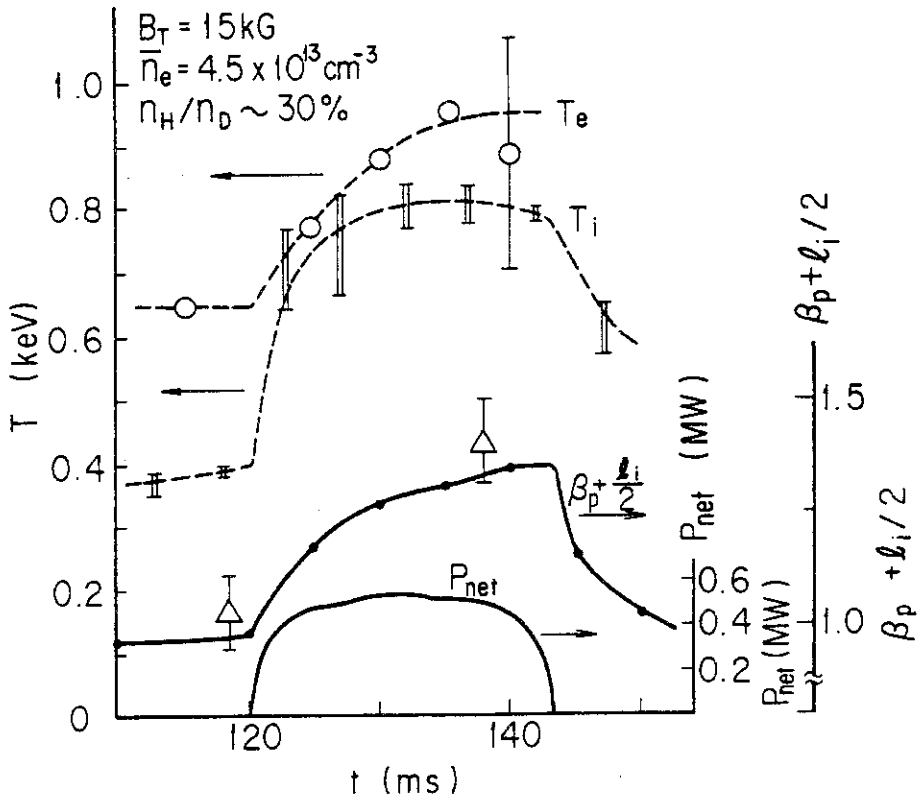

Fig. 17 (a) Time evolution of the central ion and electron temperature and $\beta p+\ell_i/2$ from the mass descriminating charge exchange analyser, laser scattering and magnetic probes, respectively. I_P=140 kA, B_T=15 kG, $n_H/n_D \simeq 30\%$ and $P_{Net} \simeq 500$kW. The triangles are from profile analysis.

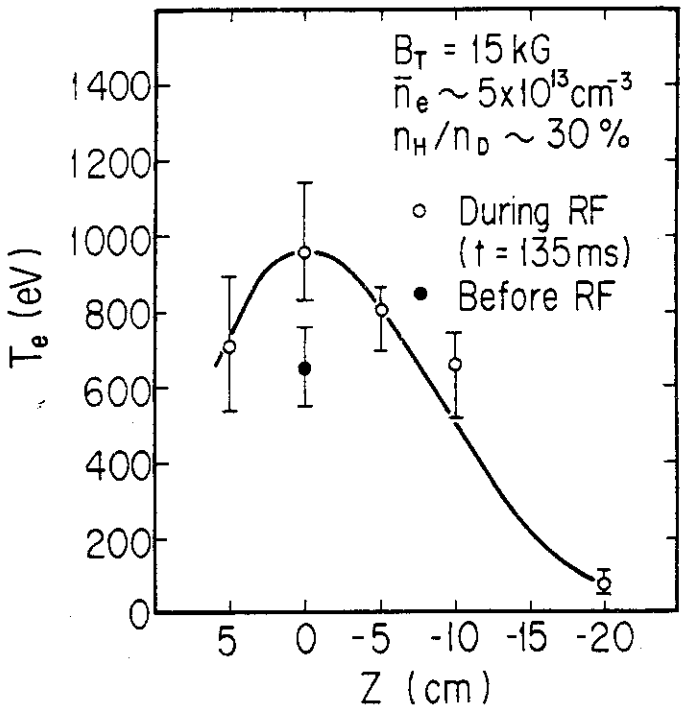

Fig. 17 (b) Vertical profile of the electron temperature during heating (open circles).

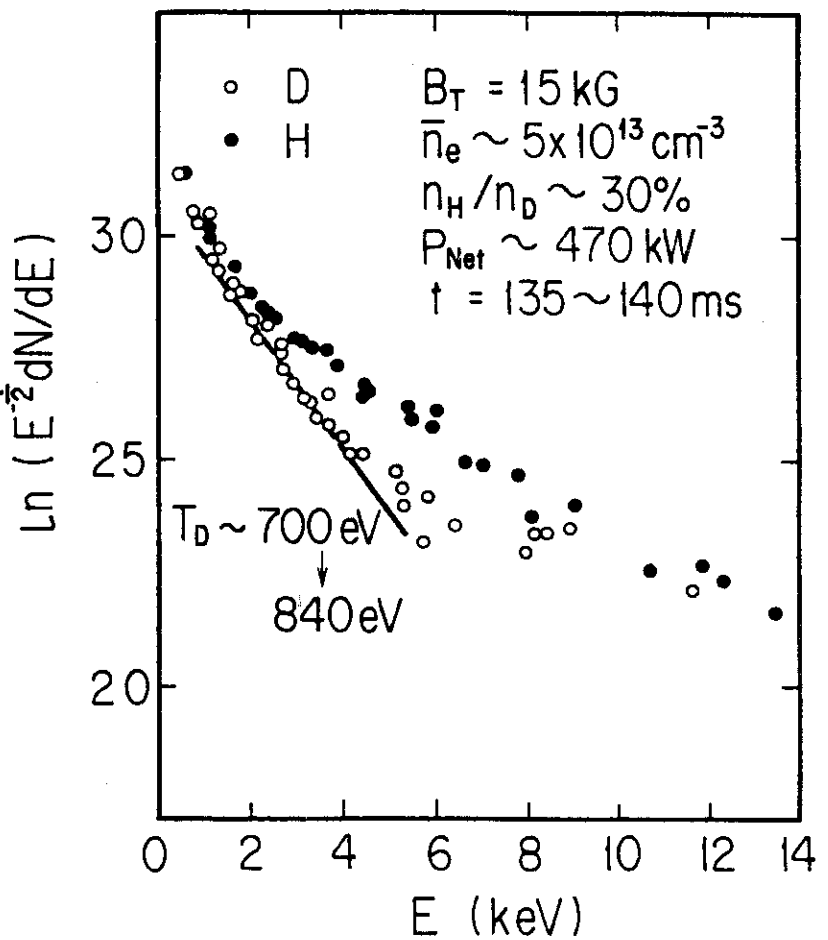

Fig. 17 (c)

Deuterium and hydrogen charge exchange energy spectra during heating.

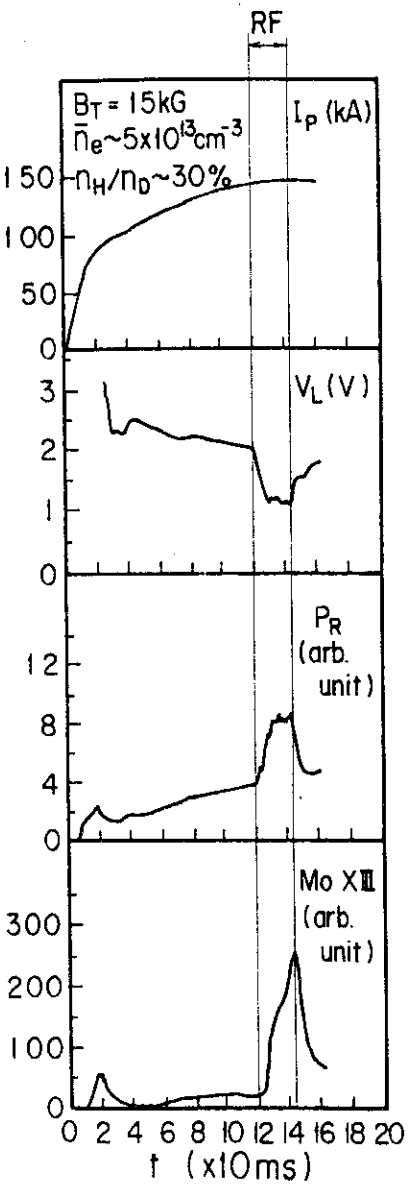

Fig. 17 (d)

Time evolution of the plasma current, loop voltage, radiation loss by the bolometer and spectral line intensity of MoXIII.

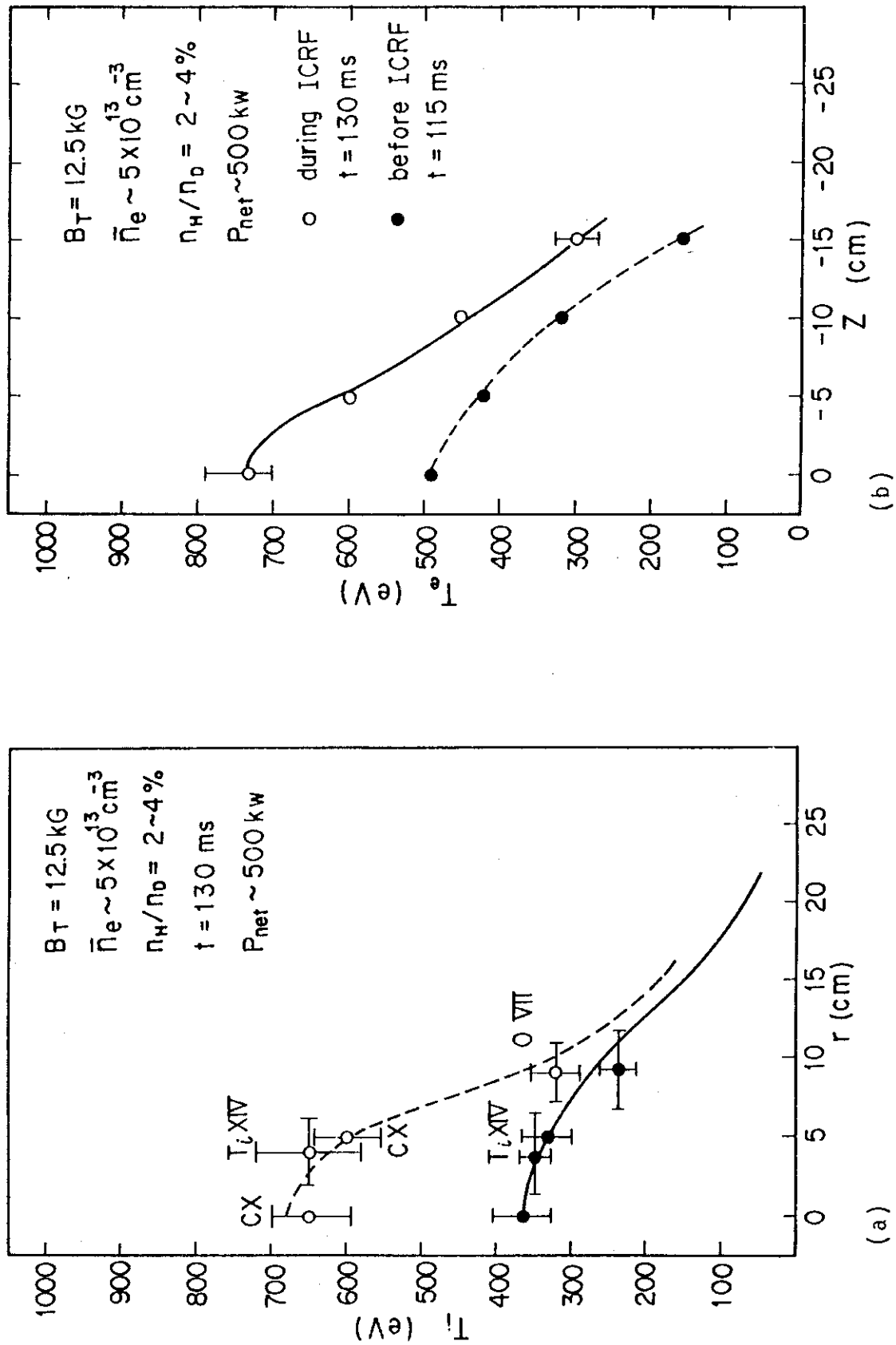

Fig. 18 Profiles of (a) ion and (b) electron temperature.
I_P=140kA, B_T=12.5kG, n_H/n_D=2∿4% and P_{Net}∿500kW.

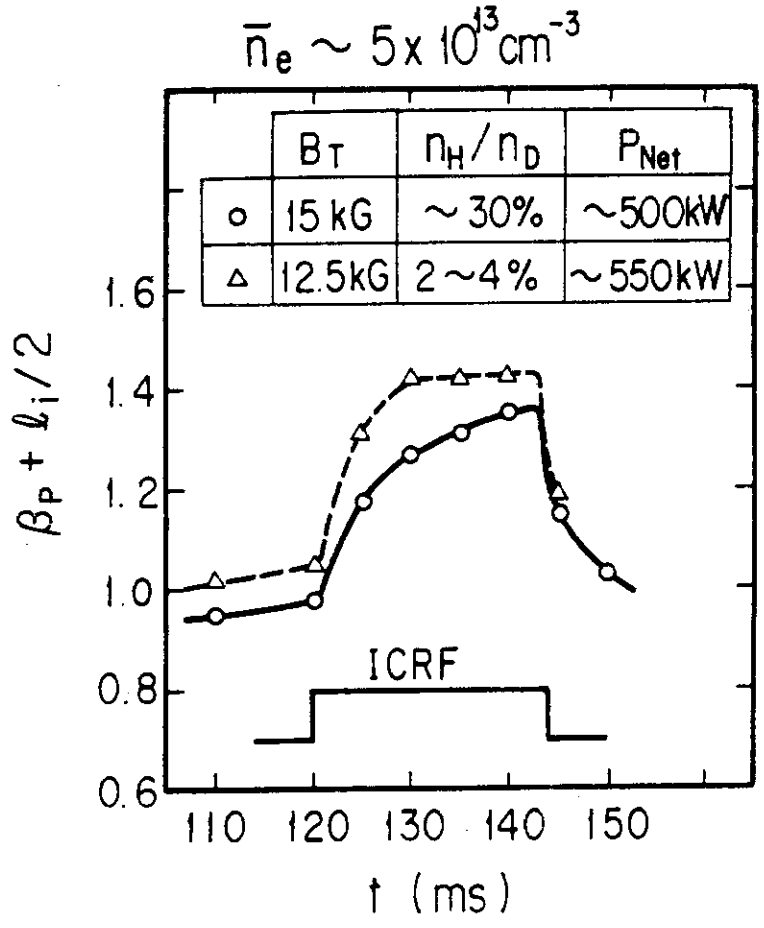

Fig. 19 Time evolution of $\beta_P+\ell_i/2$ measured by magnetics, for $n_H/n_D \sim 30\%$ (○) and $n_H/n_D = 2 \sim 4\%$ (△).